

von Freyberg, Axel ; Fischer, Andreas

### Geometric Partitioning of Complex Surface Measurements

Journal Article as: peer-reviewed accepted version (Postprint)

DOI of this document\* (secondary publication): <https://doi.org/10.26092/elib/3327>

Publication date of this document: 20/09/2024

\* for better findability or for reliable citation

#### Recommended Citation (primary publication/Version of Record) incl. DOI:

A. von Freyberg and A. Fischer, "Geometric Partitioning of Complex Surface Measurements," in IEEE Transactions on Instrumentation and Measurement, vol. 69, no. 7, pp. 4835-4842, July 2020, doi: 10.1109/TIM.2019.2954008.

Please note that the version of this document may differ from the final published version (Version of Record/primary publication) in terms of copy-editing, pagination, publication date and DOI. Please cite the version that you actually used. Before citing, you are also advised to check the publisher's website for any subsequent corrections or retractions (see also <https://retractionwatch.com/>).

© 2020 IEEE. Personal use of this material is permitted. Permission from IEEE must be obtained for all other uses, in any current or future media, including reprinting/republishing this material for advertising or promotional purposes, creating new collective works, for resale or redistribution to servers or lists, or reuse of any copyrighted component of this work in other works.

This document is made available with all rights reserved.

#### Take down policy

If you believe that this document or any material on this site infringes copyright, please contact [publizieren@suub.uni-bremen.de](mailto:publizieren@suub.uni-bremen.de) with full details and we will remove access to the material.

# Geometric Partitioning of Complex Surface Measurements

Axel von Freyberg<sup>id</sup> and Andreas Fischer<sup>id</sup>, *Member, IEEE*

**Abstract**—Dimensional inspection of microparts is challenging. Optimized processes, such as microdeep-drawing with tailored tools, even increase the requirements. While the development of fast and precise data acquisition techniques is in progress and various solutions already exist, the geometrical evaluation of measuring data still shows open questions: 1) the evaluation methods for freeform surfaces do not provide information in a form that can be directly used to assess dimensional tolerances; 2) manual association of approximating geometric elements to points is not suited for high inspection rates; and 3) partitioning based on the nominal workpiece coordinate system is affected by alignment uncertainties. An algorithm was developed for the automated evaluation of surface measuring data composed of geometric primitives, such as planes, cylinders, and tori, which combines and optimizes the estimation of geometric parameters together with the automatic partitioning of the measured points. This article presents the extension of this holistic approximation (HA) with root point iteration in order to evaluate more complex geometric elements. The verification of the extended HA for a 2-D combination of lines and an ellipse shows no systematic error and achievable uncertainties below  $0.8 \mu\text{m}$  for the approximated shape parameters of an ellipse for simulated surface data with uniformly distributed noise in the range of  $1.0 \mu\text{m}$ . The validation in comparison with commercial metrology software finally exhibits the full potential of the extended HA. As a result, a fully automatic dimensional evaluation is possible, providing geometric parameters that can directly be compared to nominal specifications and tolerances.

**Index Terms**—Automatic partitioning, combined complex geometries, holistic approximation (HA), orthogonal ellipse distance, root point iteration.

## I. INTRODUCTION

**T**HE manufacturing of high-quality products makes high demands on quality inspection. In addition, the precise inspection of dimensional microfeatures requires high-resolution data acquisition and tailored evaluation methods. The motivation of the present contribution is driven by microdeep-drawing, a sheet metal forming process for the mass production of components (which are smaller than 1 mm in at least two dimensions) for electronic devices, medical equipment, optoelectronics and sensor, or actuator

Manuscript received April 26, 2019; revised September 30, 2019; accepted November 6, 2019. Date of publication November 18, 2019; date of current version June 9, 2020. This work was supported by the Deutsche Forschungsgemeinschaft (DFG, German Research Foundation) for the Sichere Prozesse subproject B5 within the SFB 747 (Collaborative Research Center) Mikrokaltumformen—Prozesse, Charakterisierung, Optimierung. The Associate Editor coordinating the review process was Jagadeesh Kumar. (*Corresponding author: Axel von Freyberg.*)

The authors are with the Bremen Institute for Metrology, Automation and Quality Science, University of Bremen, 28359 Bremen, Germany (e-mail: a.freyberg@bimaq.de).

Color versions of one or more of the figures in this article are available online at <http://ieeexplore.ieee.org>.

technologies, such as high-precision microvalves, for use in antilock braking systems. Both the workpiece quality and the process efficiency strongly depend on the tool geometry. Within the microdeep-drawing process, the torus-shaped cutting edge was redesigned by an elliptic cross section shape, for example [1], [2], to investigate correlations of process parameters, wear mechanisms, and the product quality. The aim is an automated and precise dimensional inspection of microdeep-drawing tools. The focus lies on the quality inspection, and dimensional characterization of deep-drawing dies, whose drawing edges deviate from a circular cross section for process optimization reasons [1]. The tool quality is not only molding to the workpieces but also defines the tool life. While the precise measurement of deep-drawn microparts is still challenging, the surface measurement of the tools can be performed with sequential methods, either tactile with coordinate measuring machines (CMMs) or contour/roughness testers, or optically with point sensors. As these approaches are very time consuming, various measurement principles, such as triangulation, confocal sensors, or interferometric approaches [3] are often used, as they offer the possibility to acquire line-like (see [4]) or areal data (see [5], [6]) within short timing.

While several acquisition techniques exist for high-resolution 3-D surface measurements, the focus of this article was put on the evaluation of 3-D measurement data (according to ISO 1101), which is a combination of several geometric elements or free-form surfaces. This task requires a partitioning of the surface (ISO 17450). The evaluation of free-form surfaces, on the one hand, consists of aligning the measurement data to the nominal data of the computer-aided design [7] and to calculate and visualize the deviations of each measurement point. For this kind of quality inspection, several commercial solutions exist. Partitioning of free-form surfaces usually follows one of the approaches summarized in [8]. Beyond that, a model-based geometrical approach can be used to partition surfaces combined of geometric elements (integral elements). Like in other applications, such as the radius measurement of rotating objects with underdetermined sensor systems [9], using *a priori* knowledge to gather extra information out of the measuring data can decrease the uncertainty of the evaluation. Regarding the uncertainty of approximated features, the following relationships have to be considered during this task.

In the case of microfeatures or measurement data with a low point density, the small number of measurement points raises the uncertainty of the approximated features. The uncertainty further increases if the geometric object cannot be acquired completely. For instance, a circle segment with decreased central angle leads to increased uncertainty of the

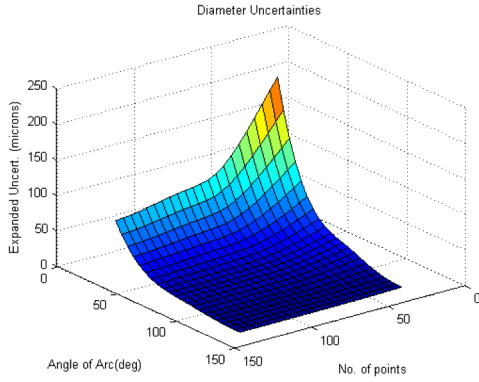


Fig. 1. Dependence of circle diameter uncertainty on the central angle (angle of arc) and the number of points [10].

approximated geometric parameters [11], [12]. Both effects are visualized in Fig. 1. A coarse rule for central angles below  $80^\circ$  is that the uncertainty of an approximated circle radius increases by a factor of 4 when the central angle is halved [10]. Therefore, as many points as possible per object should be used for precise dimensional inspection. However, a manual partitioning is time-consuming and not suitable for an automated analysis within mass production. Furthermore, the number of available points might be reduced during a manual partitioning due to a doubtful association, e.g., by leaving out points, to which a certain geometric element cannot be reliably associated. Only by an automated partitioning of the measurement data, the corresponding elements can be associated with the individual measuring points in a reproducible and optimal way. Partitioning of dimensional measurement data is very similar to the segmentation task within image processing. The methods can be divided into five classes [13]:

- 1) *Edge (Contour) Based*: Partitioning can take place based on detecting edges using different measures on neighboring pixels [14], [15] and defining them as transition zones between the segmented elements. Edge-based partitioning is fast but also very sensitive against noisy data, outliers, and uneven point densities [13]. Furthermore, assessing normal vector direction differences between neighboring points will not succeed in identifying transition borders, where two object surfaces have the same tangent planes or surface normals [16].
- 2) *Region Based*: Region-based partitioning can be performed either top-down (unseeded region) or bottom-up (seeded region). Both variants are more accurate to noise than edge-based methods, but tend to over or under segmentation and have problems to determine the region borders accurately [13].
- 3) *Attribute Clustering*: This method consists of two steps: attribute computation and clustering the points based on its attributes. Attribute clustering can be robust depending on the quality of the derived attributes [13].
- 4) *Model Based*: A problem in image segmentation is that no model can be determined *a priori* [16]. The same is valid for partitioning tasks in reverse engineering. A possible solution was introduced with the random sample consensus approach [17], which uses geometric

primitives (such as planes, spheres, or cylinders) to group the measured points. In the field of quality inspection, a geometric model exists in the form of nominal data and the defined tolerances. In general, the association of geometric elements to the measuring points is based on the nominal geometry given in the workpiece coordinate system (WCS) [10] and, thus, requires a full definition of the nominal geometry and the reference elements. During the measurement, the WCS is aligned to reference elements, which contain geometric deviations out of the production process and which are acquired with a finite uncertainty. As a result, these uncertainties of the WCS propagate to the partitioning, leading either to a certain fraction of wrong associations, or to transition zones, whose points are not considered and, therefore, cannot contribute to an evaluation with increased precision. In contrast, a holistic approximation (HA) can evaluate a composed set of data based on a geometric model in a single approximation task [18], while an optimal association of geometric elements to the corresponding measurement points (partitioning) is carried out simultaneously. A *priori* knowledge in the form of a parametric geometric model is needed, but a full definition of the nominal geometry is not required. Based on the first 2-D implementation, a 3-D application to evaluate the composition of a cylinder, a torus, and a plane is presented in [19].

- 5) *Graph Based*: Many graph-based methods use a probabilistic inference model and can be considered robust, even for complex scenes with noisy data, but they usually cannot run in real time [13]. Graph-based methods are widely used in robotics, but applications for dimensional inspections are not reported.

A newer clustering approach defines only edge detection, region growing, attribute clustering, and hybrid approaches [8], which implies defining both the model and the graph-based partitioning to be attribute clustering methods. In either way, only the HA demonstrably offers the potential for an automated optimal partitioning which is the basis for evaluating microfeatures with low uncertainties, as the maximum numbers of acquired points are associated by corresponding approximating elements. It was proven that the HA with automated partitioning is only little sensitive regarding the initial values of the approximation and at the same time converges reliably [19]. The HA is based on minimizing the orthogonal distances, which is referred to as geometric fitting, best-fit approximation or orthogonal distance regression. This method was successfully tested for the evaluation of micromerements [20], and it allows the automatic detection of outliers by a combination with statistical methods [21]. The uncertainty for approximated 3-D features was recently estimated for the HA of a combination of plane, torus, and cylinder, and validation showed submicrometer deviations for the form parameters approximated according to the geometric boundary conditions [22]. However, the HA was developed for combinations of geometric primitives, such as circles, planes, cylinders, and tori, for which the orthogonal distances to the measured points can be analytically calculated.

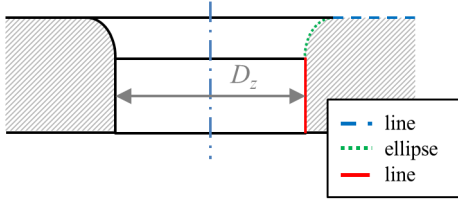


Fig. 2. Cross section of a drawing die with an elliptical drawing edge.

The quality of the dies to be inspected is defined by tolerances in the technical drawing. Thus, the nominal geometry is known and can be used for a model-based evaluation, such as HA. But, until now, geometrical compositions which contain more complex geometric elements, such as ellipses and parabolas, cannot be analyzed with this method. Thus, the extension of the HA with cascaded root point iteration (for calculating the orthogonal point distances) will be presented in this contribution in a 2-D application. Section II introduces the microdeep-drawing process and the principle of the HA with extended root point iteration. The verification results are presented and discussed in Section III, and Section IV presents the validation with experimental data. Section V closes this article with a conclusion and an outlook.

## II. METHOD AND APPLICATION

For an automated quality inspection of surface data with higher order integral elements, the HA was extended by an algorithm, which is able to calculate the orthogonal distances of the measuring points to more complex geometric elements by an iterative determination of the root points on the approximating geometric object. This article focuses on the geometric evaluation of cross sections combined of lines and ellipses. Sections II-A–II-C introduce the quality inspection task, the HA and the embedded root point iteration for the geometric combination in the addressed application.

### A. Quality Inspection of Optimized Deep-Drawing Tools

Whereas deep drawing is a well-established mass production technique in macrodimensions, size effects [23] are a general challenge in microproduction. Especially the material properties are changing with decreasing dimensions. In microforming, for example, under certain boundary conditions, the process forces increase with the grain size [24]. This is in contrast to the theory of metal forming in macro dimensions (Hall–Petch-relation) [25]. Therefore, not only the geometric inspection of the produced parts is important but also the dimensional characterization of microforming tools in order to analyze process mechanisms and to optimize friction effects.

Fig. 2 shows a cross section of a microdeep-drawing die with a hole diameter  $D_z \approx 1$  mm. Among others, the geometric features of the drawing edge influence the process, and therefore, the quality of the product. Circle-shaped cross sections of the drawing edge can be automatically analyzed with the HA. Further investigations with more complex shapes [1] shall be geometrically analyzed with an extended HA, which is introduced in Sections II-B and II-C.

This article considers a single cross section scanned by a coordinate measuring system. Each cross section represents

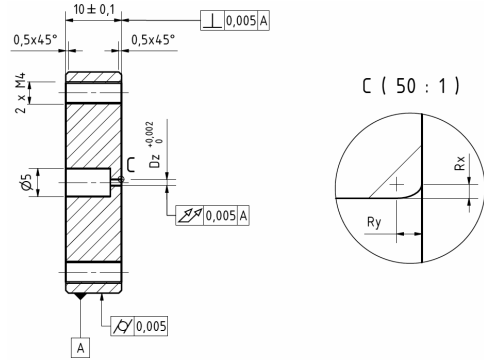


Fig. 3. Excerpt from technical drawing with nominal data and tolerances of the drawing-die. The diameter of the drawing borehole has a nominal datum  $D_z = 1.06$  mm and the two ellipse axes are defined to  $R_x = r_x = 120$   $\mu$ m and  $R_y = r_y = 150$   $\mu$ m.

TABLE I  
GCs OF THE HA MODEL

GC1	Origin of model coordinate system is in center of ellipse
GC2	Line 1 is parallel to $x'$
GC3	Minor axis of ellipse is parallel to line 1
GC4	Line 2 is perpendicular to line 1
GC5	Line 1 has distance $r_y$ to origin (tangential transition to ellipse)
GC6	Line 2 has distance $r_x$ to origin (tangential transition to ellipse)
GC7	Ellipse is defined only in quadrant 1
GC8	Line 1 is defined only in quadrant 2
GC9	Line 2 is defined only in quadrant 4

a combination of a line, a quarter ellipse, and another line. The inspection task of this contribution was to characterize the lengths of the ellipse semi-axes of the deep-drawing edge. As presented in Fig. 3, the nominal values ( $r_x = 120$   $\mu$ m and  $r_y = 150$   $\mu$ m) are defined parallel and orthogonal to the axis of the die. Therefore, the ellipse was defined as a slave element with the direction determined by the direction of line 1. Furthermore, the lines of the measured cross section are defined with certain position tolerances (see Fig. 3). Most likely, the real workpiece is manufactured with deviations from the perfect perpendicularity, which could be accounted for with an additional degree of freedom in the HA model. However, this degree of freedom was not implemented, because:

- 1) the tolerances are very narrow, and this datum was not requested to be evaluated in this inspection task;
- 2) an increasing degree of freedom negatively affects the performance of the approximation.

With these geometric constraints (GCs), which are summarized in Table I, a geometric model is derived (see Fig. 4) from the nominal geometry.

### B. Holistic Approximation and Geometric Model

The HA [18], [19] combines a geometric approximation, based on the minimization of the least squares sum

$$\min_{\mathbf{a}_p, \mathbf{a}_g} \left[ \sum_{i=1}^{n_{l1}} (d_i)^2 + \sum_{j=1}^{n_e} (d_j)^2 + \sum_{k=1}^{n_{l2}} (d_k)^2 \right] \quad (1)$$

of the orthogonal distances  $d_i$ ,  $d_j$ , and  $d_k$  from the three geometric elements (line, ellipse, and line), dependent on the transformation parameters  $\mathbf{a}_p = [\Delta x, \Delta y, \gamma]$  and the shape

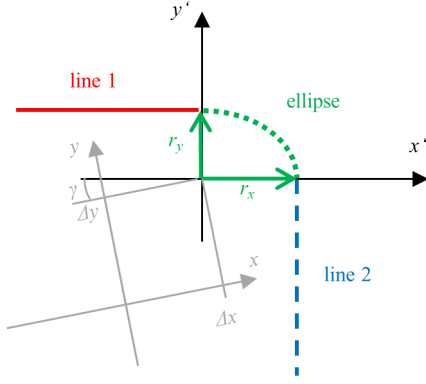


Fig. 4. Geometric model of the cross section of a drawing die as a combination of a line (red solid line), an ellipse (green dotted line; with form parameters  $r_x$  and  $r_y$ ) and another line (blue dashed line) in the MCS ( $x'$ ,  $y'$ ). The origin and the direction of the MCS are defined by a coordinate transform ( $\Delta x$ ,  $\Delta y$ ,  $\gamma$ ) with respect to the measurement coordinate system ( $x$ ,  $y$ ).

parameters  $\mathbf{a}_g = [r_x, r_y]$  with an optimal association of the geometric elements to the  $N = n_{l1} + n_e + n_{l2}$  measuring points. While the orthogonal distance can be analytically calculated for geometric primitives, such as lines, it requires the iterative determination of the root point for more complex objects, such as an ellipse. This increases the degree of freedom (DOF) of the approximation task and influences the algorithmic behavior, which is addressed in Section II-C. Here,  $n_{l1}$ ,  $n_e$ , and  $n_{l2}$  are the numbers of points to which the first line, the ellipse, and the second line, respectively, were associated. Note that these numbers change during the approximation, but they are no optimization parameters by definition. A single point has the index  $i$ ,  $j$ , and  $k$ , and its orthogonal distance to the associated geometric element  $d$  can be calculated by means of the Hessian normal forms of the lines and the parameter representation of the ellipse

$$\begin{aligned} d_i &= y'_i - r_y \\ d_k &= x'_k - r_x \\ d_j &= \begin{bmatrix} x'_i - r_x \cdot \cos(\varphi_i) \\ y'_i - r_y \cdot \sin(\varphi_i) \end{bmatrix} \end{aligned} \quad (2)$$

from the shape parameters  $\mathbf{a}_g = [r_x, r_y]$ , the angles to the ellipse root points  $\varphi_i$  and the measurement points  $\mathbf{x} = (x, y)^T$  transformed to the model coordinate system (MCS)

$$\begin{bmatrix} x' \\ y' \end{bmatrix} = \begin{bmatrix} \cos(\gamma) & \sin(\gamma) \\ -\sin(\gamma) & \cos(\gamma) \end{bmatrix} \cdot \left( \begin{bmatrix} x \\ y \end{bmatrix} - \begin{bmatrix} \Delta x \\ \Delta y \end{bmatrix} \right) \quad (3)$$

dependent on the transformation parameters  $\mathbf{a}_p = [\Delta x, \Delta y, \gamma]$ .

During the approximation, not only the free parameters are optimized but also the association of the geometric elements to the measurement points. That implies that the numbers of elements in (1) are varying during the iterative calculation. The geometric association itself is based on a geometric model, which is presented in Fig. 4. It consists of a line parallel to the  $x'$ -axis, an ellipse with radii  $r_x$  and  $r_y$ , centered in the origin of the MCS, and a second line parallel to the  $y'$ -axis. The model contains GCs derived from the workpiece design (see Fig. 3, Table I). By definition, the lines are parallel to the axes of the MCS, and the point of intersection of the two

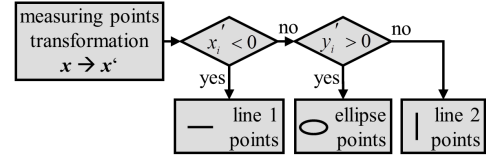


Fig. 5. Decision rules for associating the geometric objects to the measured points.

lines is shifted by  $r_x$  and  $r_y$  to the origin of the MCS, which results in a coincidence of the origin and the center of the ellipse. As a result, the DOF is the sum of 3 transformation parameters  $\mathbf{a}_p$ , two shape parameters  $\mathbf{a}_g$  and  $n_e$  additional root point positions  $\varphi_i$ .

Out of the GCs, the decision rules shown in Fig. 5 are derived and implemented in the algorithm. All transformed points with a negative  $x'$ -coordinate belong to line 1. The remaining points are distinguished by their  $y'$ -coordinate, points with positive  $y'$  are associated by the ellipse, and the residual points are associated by the second line.

### C. Root Point Iteration

Calculating the orthogonal distance for geometric objects of higher order, e.g., for an ellipse according to (2), the determination of the root points leads to  $n_e$  additional degrees of freedom. They can be calculated within the global approximation task, as proposed by Gander *et al.* [26]. However, as this approach has a bulky and sparse Jacobian Matrix and shows only a deteriorative convergence, Ahn and Rauh [27] propose a cascaded iteration. In the MCS, a point  $(x', y')$  on the ellipse can be described by

$$\begin{aligned} \frac{x'^2}{r_x^2} + \frac{y'^2}{r_y^2} &= 1 \\ \Leftrightarrow f_1(x', y') &= r_x^2 \cdot y'^2 + r_y^2 \cdot x'^2 - r_x^2 \cdot r_y^2 = 0. \end{aligned} \quad (4)$$

The implicit differentiation of 4 with  $y' = f(x')$  reads

$$0 = \frac{df_1}{dx'} = \frac{\partial f_1}{\partial x'} + \frac{\partial f_1}{\partial y'} \cdot \frac{\partial y'}{\partial x'} = \frac{-r_y'^2 \cdot x'}{r_x^2 \cdot y'} \quad (5)$$

and determines the slope  $m_t$  of the tangent at a point  $(x', y')$  on the ellipse

$$m_t = \frac{\partial y'}{\partial x'} = \frac{-r_y'^2 \cdot x'}{r_x^2 \cdot y'}. \quad (6)$$

For a measuring point  $(x'_k, y'_k)$ , the tangent line at the root point on the ellipse and the connecting line of the two points are perpendicular to each other (product of the slopes is  $-1$ )

$$\begin{aligned} m_t \cdot \frac{y'_k - y'}{x'_k - x'} &= \frac{-r_y'^2 \cdot x'}{r_x^2 \cdot y'} \cdot \frac{y'_k - y'}{x'_k - x'} = -1 \\ \Leftrightarrow f_2(x', y') &= r_y^2 \cdot x' \cdot (y'_k - y') \\ &\quad - r_x^2 \cdot y' \cdot (x'_k - x') = 0. \end{aligned} \quad (7)$$

This nonlinear root point calculation was solved by the generalized Newton method, according to [27]. As a result, this cascaded iteration delivers the root points for the measuring points associated by the ellipse, which are used by the superior HA in order to calculate the remaining free parameters, especially the shape parameters  $\mathbf{a}_g$  of the ellipse.

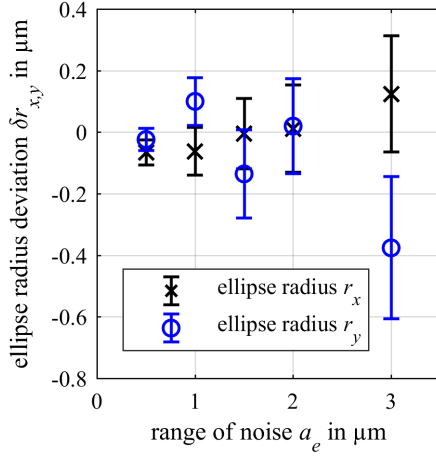


Fig. 6. Mean deviations of approximated ellipse radii  $\delta r_x = r_x - r_{(x,0)}$  and  $\delta r_y = r_y - r_{(y,0)}$  with standard errors for 100 simulated point clouds with uniformly distributed noise of different ranges  $a_e$ .

### III. VERIFICATION AND CHARACTERIZATION

For the characterization of the HA, the algorithm is assessed against the following criteria.

- 1) *Systematic Deviations*: The HA can be considered verified if no systematic influences occur.
- 2) *Random Deviations*: How does noisy data influence the algorithm?
- 3) *Optimality of Partitioning*: A decreased number of measuring points or wrong associations increase the measurement uncertainty. Only an optimal association of approximating elements to the measuring points leads to minimal uncertainty.

The geometry of the measured cross section was simulated as a combination of a line, an ellipse, and another line. The ellipse radii were defined to  $r_{x,0} = 373 \mu\text{m}$  and  $r_{y,0} = 324 \mu\text{m}$ , according to the dimensions of the application. The lateral point distance in the simulation was chosen to 0.01 mm, which is a realistic value for CMM measurements. Together with these settings, the boundaries of the simulated profile were selected in a way that all elements were formed by approximately 55 equidistant points with a uniformly distributed noise in normal direction of the nominal surface with different ranges  $[-a_e/2, a_e/2]$  in five steps between  $a_e = 0.0, \dots, 3.0 \mu\text{m}$ . Each case was simulated  $n = 100$  times and automatically evaluated by the extended HA. The initial solutions for the initialization of the minimization were randomly chosen some  $10 \mu\text{m}$  away from the defined values. The results are discussed in the following sections.

#### A. Systematic Deviations

The results of the HA of the simulated data are presented in Fig. 6. To analyze systematic deviations, an analysis of variances (ANOVA) is performed with the hypothesis  $H_0$  that the approximated radii are equal to the simulated values ( $\delta r_x = r_x - r_{(x,0)} = 0$  and  $\delta r_y = r_y - r_{(y,0)} = 0$ ) for the five simulated groups with different noise. The prerequisites of independent evaluations and Gaussian distributed random variables are fulfilled, but a Levene's test revealed that equal

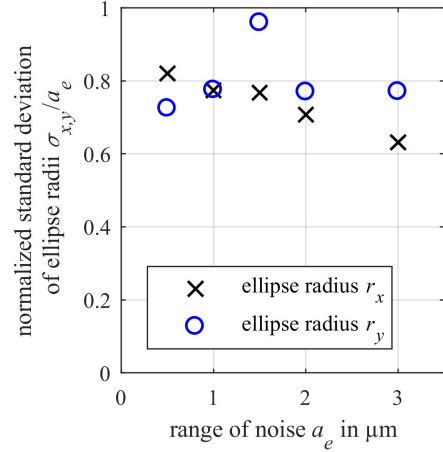


Fig. 7. Standard deviations of approximated ellipse radii  $\sigma_x$  and  $\sigma_y$ , normalized by the ranges of normal distributed noise  $a_e$  for 100 simulated point clouds.

variances could not be assumed. Therefore, a Welch ANOVA was used to analyze systematic deviations. The Welch test delivered  $F_{rx}(4; 229) = 0.34$  and  $F_{ry}(4; 222) = 1.35$ . Both values are below the critical values  $F_{crit}(0.05; 4; 229) \approx F_{crit}(0.05; 4; 222) = 2.41$ . Thus, with a probability of error of 5%, it can be assumed that no systematic influence within the HA leads to significant deviations of both approximated radii.

#### B. Random Deviations

The random deviations can be characterized by the standard deviations of the calculated radii. Fig. 7 shows the standard deviations of the approximated ellipse radii,  $\sigma_x$  and  $\sigma_y$ , respectively, normalized by the ranges of noise  $a_e$ . Within the boundary conditions of the simulations with approximately 55 points associated by the ellipse, the normalized standard deviations are between 0.6 and 1.0. This nearly constant level means the uncertainty of the algorithm is directly scaled by the range of uniformly distributed noise. The level of random deviations can be reduced if the number of measured points increases or if complete elements are evaluated. This effect can be observed in comparison with HA results in another application [22]. The normalized standard deviation of the wall radius of a partial torus, which was measured by approximately 100 000 points, was at a level of 0.4–0.5, whereas a level of 0.002 could be reached for the radius of a complete cylinder with 300 000 points.

#### C. Optimality of Partitioning

The benefit of the HA, in addition to an automated dimensional evaluation, is the optimal partitioning of point clouds. A nonoptimal partitioning leads to increased uncertainties.

- 1) Associating approximating elements to wrong points.
- 2) Ignoring points in the evaluation due to an uncertain (manual) partitioning.

To analyze the effect of wrongly associated points, combined measuring profiles were again simulated with uniformly distributed noise ( $a_e = 1.0 \mu\text{m}$ ). The automated partitioning

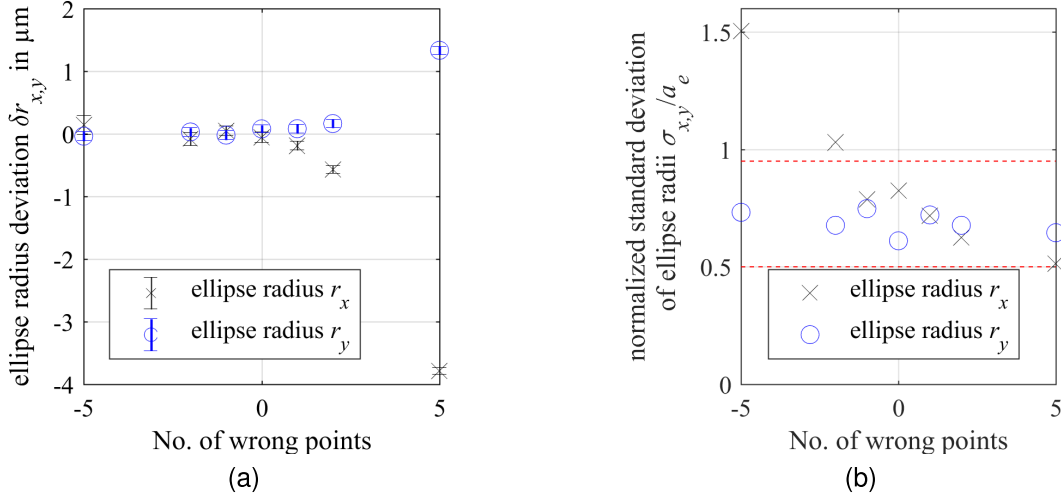


Fig. 8. Effects of wrongly associated points for 100 simulated point clouds with normal distributed noise ( $a_e = 1.0 \mu\text{m}$ ). (a) Mean deviations of approximated ellipse radii  $\delta r_x = r_x - r_{(x,0)}$  and  $\delta r_y = r_y - r_{(y,0)}$  with standard errors. (b) Normalized standard deviations of approximated ellipse radii  $\sigma_{x,y}/a_e$ .

capability of the HA was disabled, and the ellipse approximation was performed with different numbers of additional measuring points from one adjacent line in 100 repetitions in each case. The characterization results are presented in Fig. 8. It can be seen that this systematic effect increases the deviation to the nominal values for both ellipse radii with an increasing number of wrongly associated points. In this lateral measuring resolution of  $0.01 \text{ mm}$  (resulting in approximately 55 points on the ellipse), even single wrongly associated points already lead to significant systematic deviations (Fig. 8(a)).

Omitting points in the evaluation have a similar effect, which is presented in Fig. 8(b). At one end of the ellipse profile, different numbers of points were omitted in the ellipse approximation (negative number of wrong points). As a result, the random deviations (represented by the normalized standard deviation) increase for the radius  $r_x$ . A decrease in 10% (5 points) almost doubles the normalized standard deviation.

The simulation results in the preceded subsections show that the HA is neither affected by systematic effects nor shows varying dependencies on random influences. By that, it is demonstrated that the HA determines the optimal partition, which minimizes the uncertainties of the approximated geometric parameters.

#### IV. VALIDATION AND APPLICATION

For validating the HA, measurement data acquired with a CMM (Leitz Reference 10.7.6,  $\text{MPE}_p = 0.9 \mu\text{m}$ ) was evaluated and compared with the results of a reference software (Hexagon QUINDOS). The measurement was performed with a  $0.6\text{-mm}$  diameter ruby ball probe in scanning probing mode with a lateral resolution of  $1 \mu\text{m}$  (see Fig. 9). In total, 72 profiles were scanned per die in rotary steps of  $5^\circ$ .

As initial solutions for the initialization of the HA, the nominal values for the shape parameters were used and zero for the position parameters. As a result, the difference to the resulting values is in the order of some  $10 \mu\text{m}$  (form deviation and alignment error for the WCS). The results of the extended HA were compared with values calculated with reference software, which requires a manual partitioning of the measurement data.

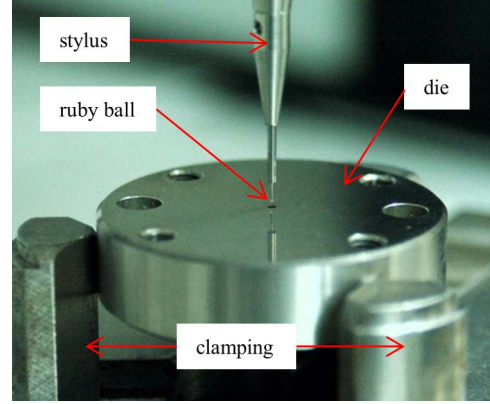


Fig. 9. CMM measurement of die with a  $0.6 \text{ mm}$  diameter ball probe, the profile to be inspected is the cross section of the central borehole.

An example of the validation is presented in Fig. 10. For direct comparability, the automatically identified ellipse points of the HA were also selected manually prior to the reference ellipse approximation. It can be observed in Fig. 10(a) that different ellipses are resulting. The reason is that in the HA, the direction of the major axis of the ellipse is defined by the geometric model. Thus, the rotation of the ellipse (in relation to the lines) as a DOF is locked in the HA. Nevertheless, in Fig. 10(b), a certain similarity is evident between the residuals of the two results. The characteristic runs of the curves result from shape deviations of the workpiece. Furthermore, the slopes at both ends indicate the transitions to the line parts of the measured profile. For example, the root-mean-square deviations (RMSD) of the HA is  $0.89 \mu\text{m}$ , whereas it is  $0.66 \mu\text{m}$  for the reference evaluation. The smaller RMSD of the reference evaluation is coherent with the additional degree of freedom, leading to a better approximation of the ellipse points. However, for the dimensional inspection according to the nominal workpiece design, the ellipse radii have to be evaluated in the direction specified in the geometric model. Here, only the values of the HA lead to a function-oriented assessment of the workpiece.

In order to demonstrate the full potential of the HA, the reference software was used for repeated manual partitioning of a measurement profile, without using the implicit partitioning of

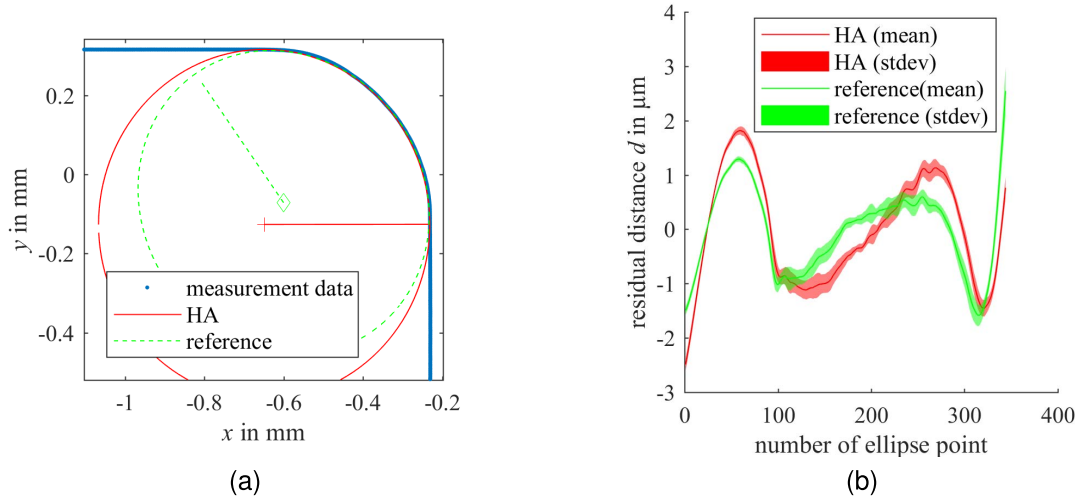


Fig. 10. Approximation results for CMM measurement data. (a) Visualization of the approximation results for HA and a manual reference evaluation for the center coordinates of the probing ball (radius: 0.3 mm). (b) Mean residual distances (for ten repeated measurements) of the measurement points to the approximating ellipses for the HA and for the reference evaluation, respectively. The confidence interval is twice the standard error.

the HA. Within ten repeated evaluations of the same measuring data, the length of the major semi-axis  $r_l$  was evaluated with a standard deviation of  $8.9 \mu\text{m}$  and a spread of  $25.4 \mu\text{m}$ , the length of the minor semi-axis  $r_s$  with a standard deviation of  $14.9 \mu\text{m}$  and a spread of  $47.6 \mu\text{m}$ . In contrast, for a repeated partitioning of one set of data, the HA delivers idem results each time. Thus, the HA shows a standard deviation of zero with respect to this significant cause of uncertainty.

The propagation of uncertainties according to supplement two of the guide to the expression of uncertainty in measurement [28] is given by

$$\mathbf{U}_d = \mathbf{C} \cdot \mathbf{U}_a \cdot \mathbf{C}^T \quad (8)$$

where  $\mathbf{U}_d$  is the covariance matrix associated with the calculated orthogonal distances,  $\mathbf{C}$  is the sensitivity matrix or the Jacobian matrix, respectively, and  $\mathbf{U}_a$  is the covariance matrix of the approximated parameter  $\mathbf{a} = (\mathbf{a}_g, \mathbf{a}_p)$ . For estimating the uncertainties of the approximated parameters, which are implicitly contained in (8), some assumptions have to be assessed, first. The coordinates acquired with a CMM are correlated, due to imperfections of the machine axes. However, by CMM calibration, these systematic influences can be reduced to an extent that can be neglected in the following considerations. Furthermore, as presented in Fig. 6, the model, on average, represents the expected (true) value. Thus, it can be assumed that:

- 1) the measurement data is uncorrelated;
- 2) the HA is an unbiased estimator.

Following the Gauß Theorem [29], also known as Gauß–Markov Theorem [30], the HA as least squares estimator is the best linear unbiased estimator. As a result, the covariance matrix of the approximated parameters

$$\mathbf{U}_a = \mathbf{C}^{-1} \cdot \mathbf{U}_d \cdot (\mathbf{C}^T)^{-1} = \sigma^2 \cdot (\mathbf{C}^T \cdot \mathbf{C})^{-1} \quad (9)$$

can be calculated from the Jacobian matrix  $\mathbf{C}$  of the least squares approximation and the uncertainty  $\sigma$  of the calculated orthogonal distances [31]. This method was also implemented in [32] to calculate the uncertainties of approximated circle

parameters in a microwave application. For the experimental results presented in Fig. 10, the empirical standard deviation  $s$  of the residual distances  $\delta_i$  of the  $n_e$  measurement points to the ellipse was used to estimate the uncertainty

$$\sigma \approx s = \sqrt{\frac{\sum_{i=1}^{n_e} \delta_i^2}{n_e - 1}}. \quad (10)$$

The estimated uncertainties of the HA for the ellipse shape parameters  $r_x$  and  $r_y$  result in  $\sigma_{r_x} = 1.21 \mu\text{m}$  and  $\sigma_{r_y} = 0.72 \mu\text{m}$ , respectively. These values are in good agreement with the standard deviation of the HA for 100 repeated evaluations of simulated measuring profiles (with uniformly distributed noise in the range  $a_e = 1.0 \mu\text{m}$ ), which is below  $0.8 \mu\text{m}$ . As a result, the uncertainty due to noise for the HA is already more than one order of magnitude smaller than only the effect of partitioning errors with the reference software.

## V. CONCLUSION

For the evaluation of measuring point clouds combined of different geometric objects, the HA offers an automated way to perform an optimal partitioning of the point clouds and, at the same time, approximate individual geometric parameters. The evaluation of geometric deviations by HA so far was only possible for combinations of geometric primitives, for which an orthogonal point distance can be directly calculated. This contribution presents an extension of the HA with an algorithm for the root point iteration, which enables the evaluation of higher order geometric objects, such as ellipses, for example.

Simulated data were used to characterize the extended HA. The statistical analysis of repeated simulation results with uniformly distributed noise showed that no systematic effects influence the approximation results (unbiased estimator). Furthermore, it was proven that random deviations of the approximation results are scaled by the range of noise of the input data and the number of measurement points. As a result, the optimal data partitioning capability of the HA was verified.

The HA was finally validated by comparing its results for CMM measurements to those of a reference software. The

reference software does not offer an automated partitioning. Therefore, the measurement data had to be partitioned manually prior to the approximation. Although the results are not directly comparable due to the boundary conditions of the HA's geometric model, they visually showed a good agreement, and the RMSD was in the same order of magnitude for both evaluations. The uncertainty of the approximated ellipse parameters was estimated to values smaller than  $1.2 \mu\text{m}$ . Finally, the validation also showed the benefit of the HA. The reference software is not capable of automated evaluation of combined surface data, and its results strongly depend on the subjective partitioning of the measuring points based on the visual assessment of the user. In contrast, the HA offers an automated evaluation and provides optimal association of the measuring points by the individual geometric objects (partitioning).

Ongoing research focuses on the 3-D implementation of the extended HA, which will provide a basis for the automated evaluation of optically acquired surface data (with parametrically defined integral geometry elements) with respect to geometric tolerances.

## REFERENCES

- [1] G. Behrens and F. Vollertsen, "Influence of tool geometry variation on the punch force in micro deep drawing," *Key Eng. Mater.*, vol. 554, pp. 1306–1311, Jun. 2013.
- [2] G. Behrens, F. O. Trier, H. Tetzl, and F. Vollertsen, "Influence of tool geometry variations on the limiting drawing ratio in micro deep drawing," *Int. J. Mater. Forming*, vol. 9, no. 2, pp. 253–258, 2016.
- [3] G. Berkovic and E. Shafir, "Optical methods for distance and displacement measurements," *Adv. Opt. Photon.*, vol. 4, no. 4, pp. 441–471, 2012.
- [4] M. M. Auerswald, A. von Freyberg, and A. Fischer, "Laser line triangulation for fast 3D measurements on large gears," *Int. J. Adv. Manuf. Technol.*, vol. 100, nos. 9–12, pp. 2423–2433, 2019.
- [5] S. Zhang, "Recent progresses on real-time 3D shape measurement using digital fringe projection techniques," *Opt. Lasers Eng.*, vol. 48, no. 2, pp. 149–158, 2010.
- [6] U. Schnars, C. Falldorf, J. Watson, and W. Jüptner, "Digital holography," in *Digital Holography and Wavefront Sensing: Principles, Techniques and Applications*. Berlin, Germany: Springer, 2015, pp. 39–68.
- [7] E. Savio, L. D. Chiffre, and R. Schmitt, "Metrology of freeform shaped parts," *Ann.-Manuf. Technol.*, vol. 56, pp. 810–835, Apr. 2007.
- [8] N. Anwer, P. J. Scott, and V. Srinivasan, "Toward a classification of partitioning operations for standardization of geometrical product specifications and verification," *Procedia CIRP*, vol. 75, pp. 325–330, 2018.
- [9] A. Fischer, "Angular-dependent radius measurements at rotating objects using underdetermined sensor systems," *IEEE Trans. Instrum. Meas.*, vol. 67, no. 2, pp. 425–430, Feb. 2018.
- [10] D. Flack, "Measurement good practice guide no. 41: CMM measurement strategies," Nat. Phys. Lab., London, U.K., Tech. Rep. 41, 2014.
- [11] P. Bourdet, C. Lartigue, and F. Leveaux, "Effects of data point distribution and mathematical model on finding the best-fit sphere to data," *Precis. Eng.*, vol. 15, no. 3, pp. 150–157, 1993.
- [12] J. I. McCool, "Systematic and random errors in least squares estimation for circular contours," *Precis. Eng.*, vol. 1, no. 4, pp. 215–220, 1979.
- [13] A. Nguyen and B. Le, "3D point cloud segmentation: A survey," in *Proc. 6th IEEE Conf. Robot., Automat. Mechatron. (RAM)*, Nov. 2013, pp. 225–230.
- [14] L. S. Davis, "A survey of edge detection techniques," *Comput. Graph. Image Process.*, vol. 4, no. 3, pp. 248–270, 1975. [Online]. Available: <http://www.sciencedirect.com/science/article/pii/0146664X7590012X>
- [15] P. J. Besl and R. C. Jain, "Segmentation through variable-order surface fitting," *IEEE Trans. Pattern Anal. Mach. Intell.*, vol. MTT-10, no. 2, pp. 167–192, Mar. 1988.
- [16] Y. Liu and Y. Xiong, "Automatic segmentation of unorganized noisy point clouds based on the Gaussian map," *Comput.-Aided Des.*, vol. 40, no. 5, pp. 576–594, 2008.
- [17] M. A. Fischler and R. Bolles, "Random sample consensus: A paradigm for model fitting with applications to image analysis and automated cartography," *Commun. ACM*, vol. 24, no. 6, pp. 381–395, 1981.
- [18] G. Goch, "Algorithm for the combined approximation of continuously differentiable profiles composed of straight lines and circle segments," *CIRP Ann.*, vol. 40, no. 1, pp. 499–502, 1991.
- [19] K. Lübke, Z. Sun, and G. Goch, "Three-dimensional holistic approximation of measured points combined with an automatic separation algorithm," *CIRP Ann.*, vol. 61, no. 1, pp. 499–502, 2012.
- [20] P. Zhang, S. Mehrafsun, K. Lübke, G. Goch, and F. Vollertsen, "Laserchemische Feinbearbeitung und Qualitätsprüfung von Mikrokaltumform-Werkzeugen," in *Kolloquium Mikroproduktion und Abschlusskolloquium SFB 499; 11.–12. Oktober 2011, Karlsruhe*, vol. 7591. Karlsruhe, Germany: KIT Scientific Publishing, 2011, pp. 169–176.
- [21] F. E. Grubbs, "Procedures for detecting outlying observations in samples," *Technometrics*, vol. 11, no. 1, pp. 1–21, 1969.
- [22] A. von Freyberg and A. Fischer, "Holistic approximation of combined surface data," *Precis. Eng.*, vol. 54, pp. 396–402, 2018.
- [23] L. V. Raulea, A. M. Goijaerts, L. E. Govaert, and F. P. T. Baaijens, "Size effects in the processing of thin metal sheets," *J. Mater. Process. Technol.*, vol. 115, no. 1, pp. 44–48, 2001.
- [24] M. Geiger, M. Kleiner, R. Eckstein, N. Tiesler, and U. Engel, "Microforming," *CIRP Ann.*, vol. 50, no. 2, pp. 445–462, 2001.
- [25] N. J. Petch, "The cleavage strength of polycrystals," *J. Iron Steel Inst.*, vol. 174, pp. 25–28, May 1953.
- [26] W. Gander, G. H. Golub, and R. Strebler, "Least-squares fitting of circles and ellipses," *BIT Numer. Math.*, vol. 34, no. 4, pp. 558–578, Dec. 1994.
- [27] S. J. Ahn and W. Rauh, "Geometric least squares fitting of circle and ellipse," *Int. J. Pattern Recognit. Artif. Intell.*, vol. 13, no. 7, pp. 987–996, 1999.
- [28] *Evaluation of Measurement Data—Supplement 2 to the 'Guide to the Expression of Uncertainty in Measurement'—Extension to Any Number of Output Quantities*, document JCGM 102, 2011.
- [29] C.-F. Gauss, *Theoria Combinationis Observationum Erroribus Minimis Obnoxiae*, vol. 1. Maingasse, Germany: Henricus Dieterich, 1823.
- [30] E. Lehmann, "A general concept of unbiasedness," *Ann. Math. Statist.*, vol. 22, no. 4, pp. 587–592, 1951.
- [31] S. M. Kay, *Fundamentals of Statistical Signal Processing*. Upper Saddle River, NJ, USA: Prentice-Hall, 1993.
- [32] I. Kása, "A circle fitting procedure and its error analysis," *IEEE Trans. Instrum. Meas.*, vol. IM-25, no. 1, pp. 8–14, Mar. 1976.

**Axel von Freyberg** was born in Bremen, Germany, in 1975. He received the Dipl.-Ing. degree in production engineering from the University of Bremen, Bremen, in 2001.

From 2001 to 2003, he was a Research Assistant with the Bremen Institute of Industrial Engineering and Applied Work Science. Since 2003, he has been the Head of the Dimensional Metrology Group, Bremen Institute for Metrology, Automation and Quality Science. He has authored 15 peer-reviewed articles, more than 30 conference contributions, and two book sections. He holds two patents. His research interests include dimensional metrology, gear metrology, and approximation theory.

**Andreas Fischer** (M'16) was born in Dresden, Germany, in 1980. He received the Dipl.-Ing. degree in electrical engineering, the Ph.D. degree in optical metrology, and the Habilitation degree from the Dresden University of Technology, Dresden, in 2004, 2009, and 2014, respectively.

From 2004 to 2005, he was a Research Assistant with the Institute of Control Theory, Dresden University of Technology, where he was a Research Assistant from 2006 to 2009 and the Head of the Measurement System Techniques Group, Laboratory for Measurement and Sensor System Techniques, from 2009 to 2016. Since 2016, he has been a Full Professor with the Production Engineering Department, University of Bremen, Bremen, Germany, where he is currently the Director of the Bremen Institute for Metrology, Automation, and Quality Science. He has authored four books or book sections, more than 70 peer-reviewed articles, and more than 120 conference contributions. His research interests include measurement system techniques, optical measurement principles for investigating production and flow processes, and the application of model-based measurement systems and their limits of measurability.